

TeaNet: universal neural network interatomic potential inspired by iterative electronic relaxations

So Takamoto* and Satoshi Izumi†

Department of Mechanical Engineering

The University of Tokyo

7-3-1 Hongo, Bunkyo-ku, Tokyo 113-8656

Ju Li‡

Department of Nuclear Science and Engineering and

Department of Materials Science and Engineering

Massachusetts Institute of Technology

Cambridge, MA 02139

A universal interatomic potential applicable to arbitrary elements and structures is urgently needed in computational materials science. Graph convolution-based neural network is a promising approach by virtue of its ability to express complex relations. Thus far, it has been thought to represent a completely different approach from physics-based interatomic potentials. In this paper, we show that these two methods can be regarded as different representations of the same tight-binding electronic relaxation framework, where atom-based and overlap integral or "bond"-based Hamiltonian information are propagated in a directional fashion. Based on this unified view, we propose a new model, named the tensor embedded atom network (TeaNet), where the stacked network model is associated with the electronic total energy relaxation calculation. Furthermore, Tersoff-style angular interaction is translated into graph convolution architecture through the incorporation of Euclidean tensor values. Our model can represent and transfer spatial information. TeaNet shows great performance in both the robustness of interatomic potentials and the expressive power of neural networks. We demonstrate that arbitrary chemistry involving the first 18 elements on the periodic table (H to Ar) can be realized by our model, including C-H molecular structures, metals, amorphous SiO₂, and water.

* takamoto.so@fml.t.u-tokyo.ac.jp

† izumi@fml.t.u-tokyo.ac.jp

‡ liju@mit.edu

I. INTRODUCTION

A universal interatomic potential (IP) with applicability to arbitrary elements, structures, transformations and chemical reactions would considerably extend the application scope of computational materials science. Currently, there are two major approaches to reaching this goal. One is to build on physics-inspired IP that has simple, closed-form expressions [1–5] and the other is to apply artificial neural networks [6–9] as neural network interatomic potential (NNIP).

Deep neural networks have proved to be successful in various machine learning tasks, including those in the fields of physics and chemistry [10–12]. After the extension of the convolution operation to the graph structure was proposed, the field of graph convolution-based neural networks (GNN) has been expanding rapidly [13–15], in particular for molecular systems, where atoms and bonds are represented by the vertices (called nodes here) and edges of the graph respectively.

Currently, however, GNN has been limited to locally stable configurations of molecular systems. A universal IP describing the potential energy landscape of chemical reaction processes such as bond formation, bond recombination, and bond breaking amongst arbitrary number of elements remains in the development stage. Also, the current GNN architecture is improved mostly by trial and error. However, inspired by the actual nonlinear iterative calculation process of density functional theory computations[16] and information flow pattern in achieving the charge-density convergence, there is a chance to improve the performance of GNN by embedding sufficient tensor-based physics into the network architecture.

First-principles calculations based on density functional theory (DFT) [16, 17] is the most reliable method for computing the reaction processes of atomic systems. The problem is the high computational cost that limits the spatial and temporal scope of such calculations. Sophisticated empirical IPs can reproduce the results of DFT calculations for 1-2 elements. For example, embedded atom method (EAM) potential incorporates the concept of electron density of metal, and Tersoff-type or modified embedded atom method (MEAM) potential incorporates the concept of bond order and angular dependence, which is derived from the tight-binding approximation of the electronic wave function, using local combination of (quasi)atomic orbitals [18]. These IPs have been widely used for simulating mechanical deformation and damage, chemical reactions, and phase transitions.

Thus far, physics-based IPs and GNN are regarded as different approaches. However, we have found that these methods can be regarded as different representations of the same tight-binding electronic relaxation framework. In other words, GNN with certain architecture can be interpreted as the physics-based model of the corresponding IPs. In this paper, we propose a NNIP form that can be considered a superset of MEAM/Tersoff potentials while mimicking electronic total-energy relaxation [16] in a local orbital (tight-binding) basis [18–20], named the tensor embedded atom network (TeaNet). In section II, we modify the architecture of GNN with new components (edge-associated in addition to node-associated variables) that fully represent the corresponding physics-based IP. Rank-2 tensors as well as vector variables are introduced in the network and the model can naturally represent propagation of orientation-dependent Hamiltonian information, that is natural in local orbital

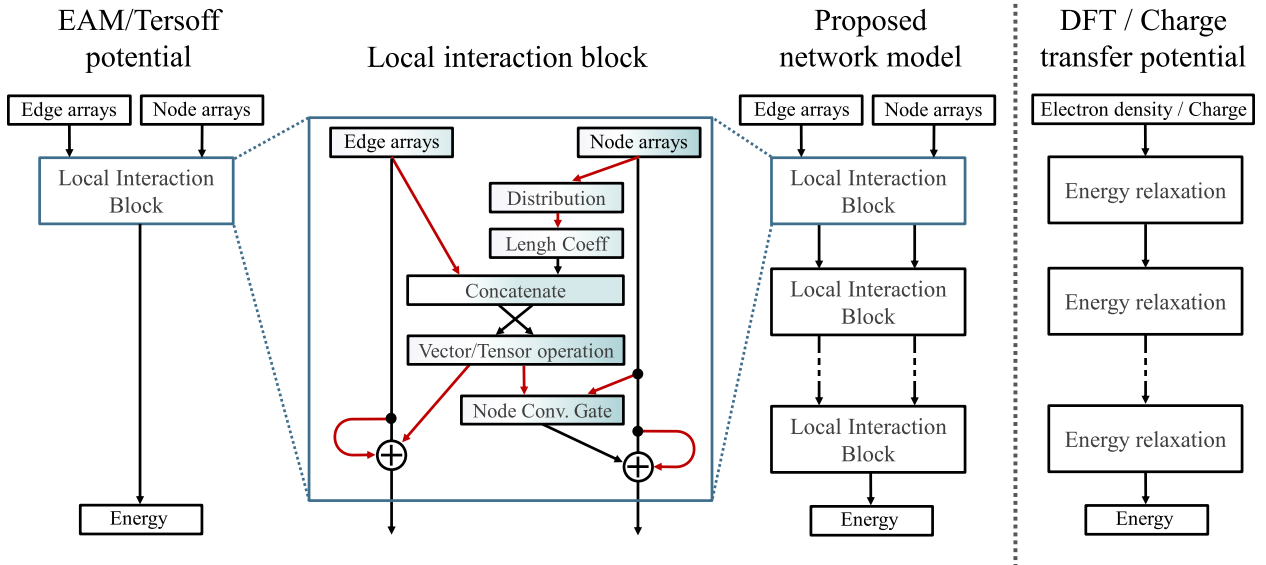


FIG. 1. Proposed network model. Linear and application functions are implemented along the red lines in the local interaction block. The light blue and dark blue in the local interaction block correspond to the vector and tensor variable values. Details are shown in section VI A.

basis calculations[18–20]. We have also adopted ResNet architecture and recurrent GNN initialization to accelerate computations.

In section III, we show the training results of our model for elements 1-18 (H-Ar) on the periodic table, where random combination of these elements in highly disordered structures are used as training set. We also performed sensitivity analysis and discussed the importance of the different features of our model. In section IV, we show the general applicability of our method in a wide range of materials including reaction processes. We demonstrate that our model performs well for liquid water, amorphous silica as well as simple metals and hydrocarbons.

II. UNIFIED VIEW OF PHYSICS-BASED IP AND GNN

Here, we show a unified view of the existing physics-based potential and GNN. We show that the governing equations underlying mainstream physics-based IPs can be effectively represented by well-designed GNN architecture. A pattern diagram of the proposed model is illustrated in Fig. 1.

In section II A, we focus on the relation between graph convolution-based local interaction and the EAM potential (corresponding left 2 diagrams in Fig. 1). Here, we rewrite EAM potential as a neural network model and point out that the single-layer graph convolution operation has the same structure as the embedding energy function of EAM potential.

In section II B, we focus on the relation between deep stacked neural network and the electronic energy relaxation procedure of the charge-transfer-type IP, which is known as charge equilibration (QEq) method[21] (corresponding right 2 diagrams in Fig. 1), as well as the iterative relaxation process in density functional theory calculations using local orbital basis. By expanding its iterative calculation, we show that the charge-transfer-type IP and charge convergence can be regarded as a restricted ResNet-style NN.

In section II C, based on the above discussions, we focus on the variable types which flow in the network. Here, we show that the Tersoff-type angular-dependent bond-order potential can also be rewritten as the graph convolution by incorporating the Euclidean tensor variables into GNN architecture. This means that the rank-2 tensor variables empower GNN to treat the spatial information naturally while keeping frame-rotation and translation invariances, in contrast to the present GNNs which use only scalar values. We also show the necessity of tensor values for transferring spatial information in graph convolution architecture.

A. Rewriting EAM potential as graph convolution

DFT calculations gain their versatility and transferability (applicability to various elements and structures) by solving the electron density over the whole space. A more approximate approach is the EAM potential [2, 22], which incorporates the concept of electron density in a shallow 1-layer network. In this popular approach, the total energy, E , is calculated as:

$$\begin{aligned} E &= \frac{1}{2} \sum_i \sum_{j \neq i} \phi_{ij}(r_{ij}) + \sum_i F_i(\rho_i), \\ \rho_i &= \sum_{j \neq i} f_j(r_{ij}), \end{aligned} \tag{1}$$

where (i, j) are the atom labels and ϕ_{ij} , F_i , f_j , and r_{ij} are functions describing the two-body energy, the embedding energy, the electron charge, and the interatomic distance, respectively. The function ρ_i , corresponding to the background electron density at atom i , can be expressed as a single-layer graph convolution (see Fig. 2).

From the view of graph convolution network, the EAM potential can be described as follows: The atomic information (on the nodes) is distributed to the corresponding edges (r_{ij}). Then, the edge-related values ($\phi_{ij}(r_{ij})$, $f_i(r_{ij})$) are calculated. A part of them ($f_i(r_{ij})$) are summed to the corresponding nodes and node-site nonlinear function ($F_i(\rho)$) is applied. In this work, we call the embedding function $F_i(\rho)$ the node gate function. The graph convolution operation of our proposed model is based on this network (“Local interaction block” in Fig. 1). The main difference, “Vector/Tensor propagation”, is described in section II C.

It is noted that EAM potential has the required invariances such as permutation, pair order, and isometry. To accumulate the edge information ($f_j(r_{ij})$) into nodes, the node gate function (F_i) plays an important role. In EAM potential, F_i represents the interaction between certain atoms and the surrounding electron density. Therefore, from a physics standpoint, the node gate function is essential in the network architecture. The node gate function’s effect on

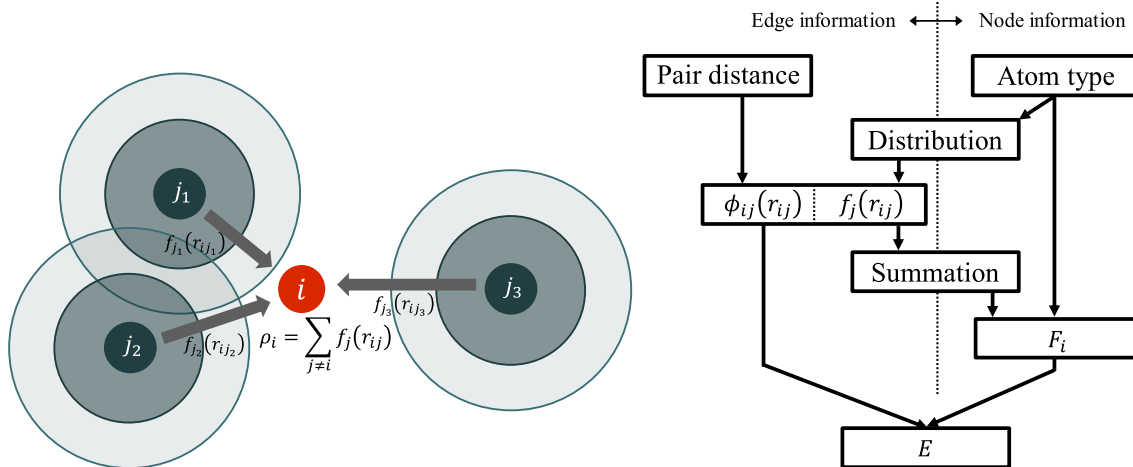


FIG. 2. EAM potential represented as a graph convolution. Left: Schematic of the summation operation. Right: Corresponding network model.

prediction accuracy is presented in section III.

B. Seeing the iterative electronic energy minimization process as a stacked neural network model

Although EAM potential incorporates the concept of electron density, it is calculated in one shot. This means that although the electron states are assumed to be determinable only by local information, this assumption is actually not physically correct, as seen by the long-ranged nature of the dielectric response function in DFT[23]. The long-range charge transfer effect plays important roles in chemical reactions. DFT calculates the ground state of the electron density by an iterative procedure. To incorporate such long-ranged propagation of information, charge-transfer-type IPs [21, 24–26], which model the deviation of the electron density and minimize the energy of the system with respect to the charge distribution, are being actively developed. The energy minimization involves implicit matrix-vector equations solved by matrix inverse calculation [21, 24] or solved by repeatedly updating the charge distribution using the gradient-based Krylov subspace method [25]. If the number of iterations is fixed, this iterative procedure could be written as a feed-forward data flow model.

The residual network (ResNet) [27] and its derivatives [28–30] have recently emerged in the fields of image recognition, as have other machine-learning tasks, including object detection [31], machine translation [32], and speech synthesis [33]. ResNet’s core idea is to “bypass” the output values from the middle layers and add them directly to the lower layer to avoid gradient disappearance during back propagation. Interestingly, previous studies interpreted the ResNet architecture as an explicit Euler method of ordinary and partial differential equations [34–36]. This indicates that stacking the local interaction block with a ResNet structure can express the energy minimization procedure of the charge-transfer type of interatomic potentials.

It is noted that iterative total energy minimization reproduces the physically reasonable long-range interactions. A well-known example is the Green’s function solution that can be represented by a matrix-vector equation $\mathbf{Ax} = \mathbf{b}$: even though \mathbf{A} is a sparse matrix (local interactions), the inverse \mathbf{A}^{-1} is dense and resembles long-range interactions. However, by iteratively solving $\mathbf{Ax} = \mathbf{b}$ with Krylov subspace method $\{\mathbf{b}, \mathbf{Ab}, \mathbf{A}^2\mathbf{b}, \mathbf{A}^3\mathbf{b}, \dots, \mathbf{A}^n\mathbf{b}\}$, one can achieve excellent approximant to the long-range interaction, which is akin to an n -layer neural network with identical weights (recursive neural network).

This analogy is useful for training procedures as well as for determining the network architecture. Since all middle layers of the energy minimization process are the same as each other, it is reasonable to make a constraint that all middle layers have the same NN parameters. This greatly improves the stability at the initial stage of training. One can find similarities to the recurrent GNN architecture [13]. This constraint is eliminated after the initial training. The physics and mechanics analogy is to use the same Green’s function response as the first-approximation in a heterogeneous and time-dependent medium, to improve the stability and convergence, before incorporating these heterogeneities in more refined calculations.

C. Translating bond angle interaction into graph convolution and embedding vector and tensor values

Another challenge to be tackled is the angular dependence [3]. Generally speaking, atomic interactions depend on the bond angle between interacting atoms. For example, H_2O and NH_3 molecules are stabilized at a certain bond angle. Diamond comprises a tetrahedral network. These angular dependencies are generated by the interaction between electron orbitals [18].

When embedding spatial information in the network architecture, satisfying invariance requirements can be challenging. The energy should be invariant to the rotation of the basis vectors. Invariance is handled differently in different models. One solution is to limit the input data to only the bond length. SchNet [9] and PhysNet [37] uses bond length only. Deep tensor neural networks (DTNN) [8] and deep potential molecular dynamics (DPMD) [38] also maintain the rotational invariance by using bond length. However, if the angle information is lacking, the model would not easily reproduce angular-dependent phenomena. Since the solution of using the raw values of vector components as the input values loses the rotation invariance, it is not appropriate for a molecular dynamics simulation.

Many existing IPs involve bond angles directly. For example, the Stillinger-Weber potential [3] has a three-body energy function. Bond-order-type potentials, such as the Tersoff potential [4, 39], possess a bond-order term consisting of the three-body angular-dependent term. Some machine learning-based models give similar solutions. The Behler-Parrinello neural network (BPNN) [6] calculates the three-body symmetry functions.

However, the bond angles correspond to neither nodes nor edges but rather to three-body atom combinations. Therefore, they should be combined and converted into representative node and edge values during the convolution operation, which requires the use of ad-hoc functions such as symmetry functions. Another problem is the lack of long-range interaction

in the three-body angle term. In GNN, local information can transfer to farther nodes through the convolutional layers. Transfer of the angle information is also desirable. For example, the directional electronic orbitals of the π bonds can be extensively spread. However, convolution of the angular information at the node crushes the angle information and prevents its propagation.

Here, we show that the angle-dependent three-body convolution algorithm can be naturally expressed as a normal node-and-edge convolution operation using Euclidean vector and second-order tensor values. This means that the model can have local spatial information and propagate it to farther nodes, and to interact with them at nodes while keeping rotational invariances. This is achieved by rewriting the Tersoff-type angle-dependent bond-order function as a convolution operation.

The Tersoff-type angle-dependent term ζ_{ij} can be written as

$$\begin{aligned} E &= \frac{1}{2} \sum_{i,j \neq i} \phi_A(r_{ij}) + \frac{1}{2} \sum_{i,j \neq i} b(\zeta_{ij}) \phi_B(r_{ij}), \\ \zeta_{ij} &= \sum_{k \neq i,j} G(\theta_{ijk}) H(r_{ij}, r_{ik}), \end{aligned} \tag{2}$$

where i , j , and k are the atom labels; θ_{ijk} is the angle between bonds ij and ik ; r_{ij} and r_{ik} are the bond lengths, and ϕ_A , ϕ_B , b , G , and H are various functions. In some Tersoff-type potentials [5, 26], the ζ_{ij} term is expressed as

$$\zeta_{ij} = \sum_{k \neq i,j} [c + d \{h - \cos(\theta_{ijk})\}^2] f_c(r_{ik}) \exp[\lambda(r_{ij} - r_{ik})], \tag{3}$$

where f_c is the cutoff function and c , d , h , and λ are the parameters. After expanding the

factors and converting the parameters, Eq. (3) is transformed to

$$\begin{aligned}
\zeta_{ij} &= \exp(\lambda r_{ij}) \sum_{k \neq i, j} [g_0 + g_1 \cos(\theta_{ijk}) + g_2 \cos^2(\theta_{ijk})] f_c(r_{ik}) \exp(-\lambda r_{ik}) \\
&= \exp(\lambda r_{ij}) \sum_{k \neq i, j} [g_0 + g_1 \hat{\mathbf{r}}_{ij} \cdot \hat{\mathbf{r}}_{ik} + g_2 (\hat{\mathbf{r}}_{ij} \cdot \hat{\mathbf{r}}_{ik})^2] f_c(r_{ik}) \exp(-\lambda r_{ik}) \\
&= \exp(\lambda r_{ij}) \sum_{k \neq i, j} [g_0 + g_1 \hat{\mathbf{r}}_{ij} \cdot \hat{\mathbf{r}}_{ik} + g_2 (\hat{\mathbf{r}}_{ij} \otimes \hat{\mathbf{r}}_{ij}) : (\hat{\mathbf{r}}_{ik} \otimes \hat{\mathbf{r}}_{ik})] f_c(r_{ik}) \exp(-\lambda r_{ik}) \\
&= \exp(\lambda r_{ij}) \sum_{k \neq i} [g_0 + g_1 \hat{\mathbf{r}}_{ij} \cdot \hat{\mathbf{r}}_{ik} + g_2 (\hat{\mathbf{r}}_{ij} \otimes \hat{\mathbf{r}}_{ij}) : (\hat{\mathbf{r}}_{ik} \otimes \hat{\mathbf{r}}_{ik})] f_c(r_{ik}) \exp(-\lambda r_{ik}) \\
&\quad - (g_0 + g_1 + g_2) f_c(r_{ij}) \\
&= g_0 \exp(\lambda r_{ij}) \left[\sum_{k \neq i} f_c(r_{ik}) \exp(-\lambda r_{ik}) \right] \\
&\quad + g_1 \exp(\lambda r_{ij}) \hat{\mathbf{r}}_{ij} \cdot \left[\sum_{k \neq i} \hat{\mathbf{r}}_{ik} f_c(r_{ik}) \exp(-\lambda r_{ik}) \right] \\
&\quad + g_2 \exp(\lambda r_{ij}) (\hat{\mathbf{r}}_{ij} \otimes \hat{\mathbf{r}}_{ij}) : \left[\sum_{k \neq i} (\hat{\mathbf{r}}_{ik} \otimes \hat{\mathbf{r}}_{ik}) f_c(r_{ik}) \exp(-\lambda r_{ik}) \right] \\
&\quad - (g_0 + g_1 + g_2) f_c(r_{ij}),
\end{aligned} \tag{4}$$

where $\hat{\mathbf{r}}_{ij}$ and $\hat{\mathbf{r}}_{ik}$ are the unit vectors. The symbols “ \cdot ,” “ $:$,” and “ \otimes ” denote the inner product, the Frobenius inner product, and the tensor product (dyad) of two vectors, respectively. Since all summation terms are written without j , they can be calculated by the convolution operation. As a result, the Tersoff-type potential function can be written as a two-layered neural network. The necessity of the Rank-2 tensors for the angle interaction using convolution operation and its physical meaning are shown in the Appendix.

Based on this discussion, we introduce both vectors and tensors into the network. Each node array contains scalar, vector, and tensor values, whereas each edge array contains scalar and vector values. A relative position vector is also provided as an input value. The effects of tensor values on prediction accuracy are presented in the section III. See section VI A for the details of the implementation.

III. TRAINING PROCEDURE AND RESULTS

A. Dependence of accuracy on the number of NN layers

There are several datasets for atomic systems, without reaction barrier information. For example, QM7 (GDB7-12) [40] and QM9 (GDB9-14) [41] are composed of equilibrium

TABLE I. Regression accuracy of trained networks with various numbers of layers.

# layers	# params	Test loss function [unitless]	Energy MAE [meV/atom]	Force MAE [eV/Å]
2	87,000	2.54	32.5	0.213
4	235,000	1.92	23.9	0.167
8	529,000	1.65	21.4	0.143
16	1,120,000	1.62	19.3	0.142

molecular data. In contrast, to reproduce reaction barriers, the model should reproduce a wide range of structures. Therefore, evaluations of highly disordered structures including dangling bonds, overcoordinated atoms, and various disordered bond lengths are required. Therefore, we prepare our own dataset of highly disordered structures using molecular dynamics simulations. The dataset consists of the first three rows of the periodic table (from H to Ar). The details of the data preparation are shown in section VI B.

We trained networks of different depths (2, 4, 8, and 16 layers). The hyperparameters and other settings for training are shown in section VI C. The results are depicted in Table I. Increasing the number of layers improved the network accuracy. No overfitting was observed in any system. In the best-performing network (with 16 layers), the mean absolute error (MAE) of the energy was 19.3 meV/atom, which is comparable to the chemical accuracy limit (1 kcal/mol \simeq 43 meV/atom).

Although our aim is to reproduce the potential energy of highly disordered atomic configurations, we also evaluated our model for datasets of locally stable atomic configurations. First, the QM9 dataset was used. Since QM9 contains only stable structures, it is possible to increase accuracy by retraining. We retrained the four-layer version of the network with the stochastic gradient descent (SGD) optimizer while gradually decreasing the learning rate. The mean squared error of the energy was used as the loss. In this case, we use the original QM9 validation dataset as the test dataset. The MAE of the energy was 13 meV per molecule (1.2 meV/atom) among the QM9 validation dataset. This is similar to the current top scores (14 meV [9], 8 meV [37]), and the other methods (19-130 meV) [7]. It is noted that the error of the dataset with locally stable structures is one magnitude smaller than that of highly disordered structures shown in Table I.

Second, the Materials Project molecule dataset, which consists of elements in the first three rows of the periodic table, was used. We recalculated the energy of the dataset by DFT to adjust the difference in the method of DFT. We trained the network in the same way as with QM9. The resulting MAE of the energy was 3.1 meV/atom. Our model well succeeds in estimating the energy of locally stable atomic configurations. It is noted that our model does not require the bond types as the input and that we use a relatively short cutoff distances (6 Å).

TABLE II. Comparison between the baseline and the four-layer network with one removed component.

	Test loss function	Energy MAE [meV/atom]	Force MAE [eV/Å]
Original four layers	1.84	22.6	0.161
w/o tensor	2.15	25.5	0.190
w/o gate	1.99	24.5	0.174
Softplus	1.89	24.1	0.165

B. Effects of the proposed components of the network

To investigate the effects of the components in our proposed network architecture, we systematically removed their corresponding functions and checked each component effect. The results are presented in Table II.

First, the network was run without inputting the tensor values (“w/o tensor” row in Table II). To conduct a fair test, the number of scalar values was increased to maintain the original number of parameters in the network. Then, the network was run without the node convolution gate (“w/o gate” row in Table II). The number of scalar values was again increased to offset the reduction in the number of parameters. Finally, the proposed activation function was replaced by the softplus function (“Softplus” row in Table II). A four-layer network without the initial 450,000 iterations was used for comparison.

The largest decrease in accuracy is seen in the case without a tensor value. The second largest decrease is in the case where the node convolution gate was not inserted. Interestingly, the proposed activation function outperformed the softplus function.

IV. MATERIALS APPLICATIONS

A. Overview

The universal NNIP should be applicable to arbitrary 3D atomic configurations with any bond types, crystal/molecular structures, and element type (up to Ar in this dataset). We have tested various systems including molecular systems, inorganic crystal structures, water, and aqueous solutions.

In this section, we used the four-layer version of the neural network in consideration of the calculation cost of MD simulations. This is like the embedded-atom potential with embedding applied four times, and with tensors and vectors propagating inside as well.

B. Intramolecular structure

We tested the reproducibility of the structures of small C-H molecules. The bond lengths and bond angles of typical small hydrocarbon molecules were compared, and the results are listed in Table IV C.

Our model can reproduce both the bond lengths and angles with good accuracy. In particular, a variety of C-C bonding (*sp*, *sp*², and *sp*³) is well reproduced. It is noted that ethene forms a planar structure and that ethane forms a staggered conformation. This indicates that our model captures the dihedral angle (4-node) interactions by passing vector and tensor information through the C-C bond. In addition, we confirmed that benzene forms a planar structure while cyclohexene forms a chair-type structure, which is a typical difference in bonding nature between aromaticity and a single bond.

C. Bulk properties of metal and semiconductor

Metals have delocalized dielectric response, while materials with bandgap can have exponentially localized response [18]. Table IV C shows TeaNet predictions of Na, Al, and Si. Several crystal structure polymorphs of the same element were evaluated.

D. Amorphous silicon dioxide

Since SiO₂ amorphous structure has various bond angles and various coordination numbers, it is treated as a benchmark of the IPs [26, 42]. Amorphous SiO₂ configuration including 648 atoms is obtained by a melt-quench process. The obtained structure and the partial radial distribution functions are shown in Fig. 3. The result is in good agreement with those of previous studies [26, 43].

E. Properties of water

Water is ubiquitous in chemistry and biochemistry. Atomistic simulation of polar and protic solvent is, therefore, essential for chemistry, biochemistry and electrochemistry. First, the ice (ice Ih) crystal structure was created. The calculated density of ice at 200 K was 0.93 g/cm³. Second, liquid properties were investigated. As an initial structure, an MD cell having 512 H₂O molecules was prepared. It was melted at 800 K for 1 ps under NVT ensemble and then annealed at 300 K and 1 bar for 3 ns under NPT ensemble. The density of liquid water was 1.00 g/cm³. These values are in good agreement with the experimental values (0.92 g/cm³ at 200 K, 1.00 g/cm³ at 300 K), and we confirmed that the density of water is higher than that of ice [45]. Figure 3 shows a snapshot of TeaNet simulation of a system of water molecules at

TABLE III. Top: Structural accuracy on small hydrocarbon molecules. Bottom: calculated lattice constants and cohesive energies of different phases of Na, Al, and Si. The cohesive energies corresponding to the most stable structure are shown in bold.

	C-C length [Å]		C-H length [Å]		H-C-C angle [degree]	
	DFT	TeaNet	DFT	TeaNet	DFT	TeaNet
Acetylene (C ₂ H ₂)	1.21	1.21	1.07	1.06	180°	180°
Ethene (C ₂ H ₄)	1.33	1.34	1.09	1.09	122°	121°
Ethane (C ₂ H ₆)	1.53	1.53	1.10	1.10	112°	112°
Benzene (C ₆ H ₆)	1.40	1.40	1.09	1.09	120°	120°
Cyclohexene (C ₆ H ₁₂)	1.53	1.55	1.10	1.10	110°	110°

	Lattice constant [Å]		Cohesive energy [eV/atom]	
	DFT	TeaNet	DFT	TeaNet
Na FCC	5.30	5.39	1.10	1.16
BCC	4.22	4.30	1.09	1.15
Diamond	7.62	7.29	0.76	0.77
Al FCC	4.05	4.11	3.42	3.43
BCC	3.23	3.26	3.27	3.38
Diamond	6.05	6.30	2.79	2.75
Si FCC	3.91	4.26	3.97	4.43
BCC	3.17	3.37	3.93	4.40
Diamond	5.47	5.47	4.64	4.76

300 K, and the partial radial distribution function of water predicted by our model compared to the experiment [44].

Another important property of water is its high dielectric constant. In MD simulation, the dielectric constant ϵ can be calculated from the fluctuation of the total dipole moment by [46]

$$\epsilon = 1 + \frac{4\pi}{3Vk_{\text{B}}T} (\langle M^2 \rangle - \langle M \rangle^2), \quad (5)$$

where M , V , k_{B} , and T are the dipole moment, volume, Boltzmann constant, and temperature, respectively. $\langle \rangle$ corresponds to the time average operation. The dipole moment of a single H₂O molecule is set to 1.8546 Debye in this simulation. The calculated dielectric constant was around 52 (Experimental value: 78 at 298 K [45]).

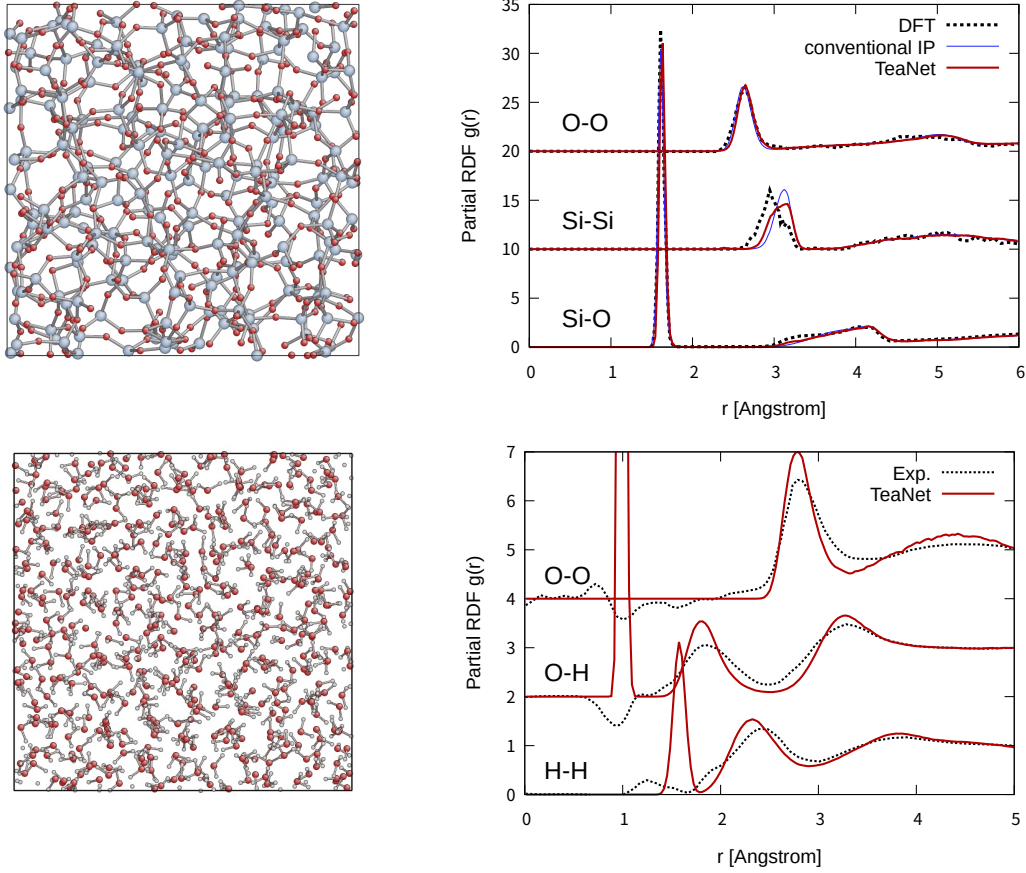


FIG. 3. Top left: obtained SiO_2 amorphous structure. Top right: comparison of partial radial distribution function of amorphous SiO_2 with DFT[43] and conventional IP[26]. Bottom left: snapshot of water. Bottom right: partial radial distribution function of water at 300 K. The experimental data is derived from the merged X-ray and neutron scattering data [44]. It is noted that the first peaks of O-H and H-H in this work correspond to intramolecular bonds.

F. Ion dissociation and the Grotthuss proton diffusion mechanism

Next, we investigate ion dissociation, proton transport, and the Grotthuss mechanism by simulating HCl in H_2O . As a result, the HCl molecule dissociated and a single Cl atom and H_3O molecule were created. Here, Cl and H_3O are shown without $+/-$ signs because the charge deviation effect cannot be extracted explicitly. After this, occasionally one H atom in the H_3O was observed to hop to another neighboring O atom, as shown in Figure 4. This proton transfer process, known as the Grotthuss mechanism, plays an important role in proton diffusion. But previously there was no bonded IP that can reproduce the Grotthuss mechanism. In TeaNet MD, the calculated effective diffusion coefficient of H_3O is $1.5 \times 10^{-6} \text{ cm}^2/\text{s}$, which is in good agreement with the previous DFT study (DFT: $1.3 \times 10^{-6} \text{ cm}^2/\text{s}$ at 300 K [47]).

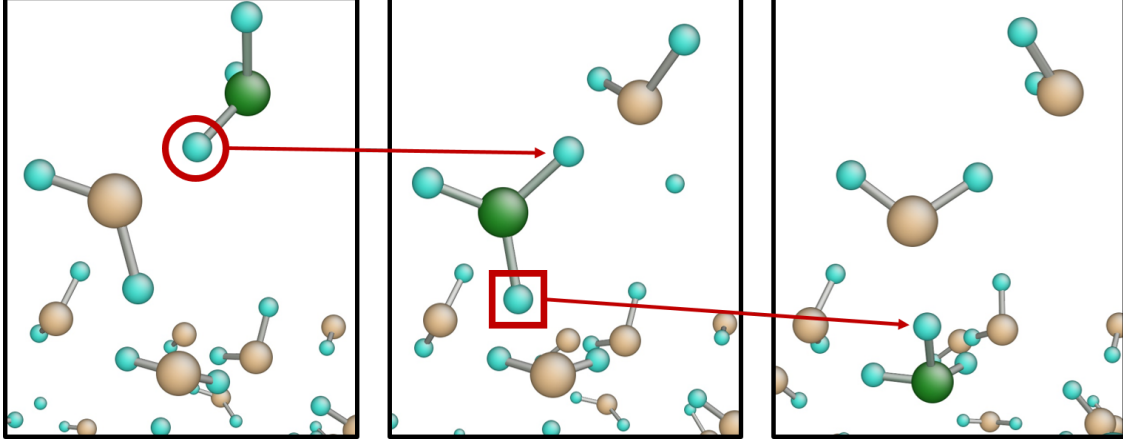


FIG. 4. Snapshots of hopping of H between H_2O molecules. H, 2-coordinate O, and 3-coordinate O are shown by blue, yellow, and green spheres, respectively. (Left): In water, H in H_2O and H_3O are oriented to neighboring O atoms. (Left to middle): An H in H_3O hopped to another O. (Middle to right): Another H in the H_3O molecule hopped to the other H_2O molecule. As a whole, these events were considered as the Grotthuss diffusion of H.

V. CONCLUSION

In this paper, we provided a unified view of GNN and physics-based interatomic potentials. Based on the findings, we proposed a new network model, named the tensor embedded atom network (TeaNet). In this network, the graph convolution is associated with EAM potential and the stacked network model is associated with the iterative electronic total energy relaxation calculation. The Euclidean vectors and tensor values are incorporated into the model to reproduce the propagation of orientation-dependent Hamiltonian information. TeaNet mimics the information flow of nonlinear iterative electronic relaxations (truncating at 5 iterations at present). The proposed model shows great performance for the first 18 elements on the periodic table (H to Ar) even for highly disordered structures. We showed that it can reproduce a diverse range of material properties including C-H molecular structures, metals, amorphous SiO_2 , liquid water and ice.

VI. METHODS

A. Specification of network

The details of the TeaNet variable flow are as follows. Here, \mathbf{n}_s , \mathbf{n}_v , and \mathbf{n}_t correspond to node scalar, node vector, and node rank-2 tensor arrays, respectively. It is noted that each variable is also an array and has multiple values per node or edge. For example, if the system has 10 atoms and the length of the array of \mathbf{n}_v is set to 16, the shape of total \mathbf{n}_v will be 10

TABLE IV. List of the input values of \mathbf{n}_s .

Element	\mathbf{n}_s
H	[0.5, 0, 0, 0, 0, 0, 0, 0, 0]
He	[1, 0, 0, 0, 0, 0, 0, 0, 0]
Li	[1, 0.5, 0, 0, 0, 0, 0, 0, 0]
Be	[1, 1, 0, 0, 0, 0, 0, 0, 0]
B	[1, 1, 0.5, 0, 0, 0, 0, 0, 0]
C	[1, 1, 1, 0, 0, 0, 0, 0, 0]
N	[1, 1, 1, 0.5, 0, 0, 0, 0, 0]
O	[1, 1, 1, 1, 0, 0, 0, 0, 0]
F	[1, 1, 1, 1, 0.5, 0, 0, 0, 0]
Ne	[1, 1, 1, 1, 1, 0, 0, 0, 0]
Na	[1, 1, 1, 1, 1, 0.5, 0, 0, 0]
Mg	[1, 1, 1, 1, 1, 1, 0, 0, 0]
Al	[1, 1, 1, 1, 1, 1, 0.5, 0, 0]
Si	[1, 1, 1, 1, 1, 1, 1, 0, 0]
P	[1, 1, 1, 1, 1, 1, 1, 0.5, 0]
S	[1, 1, 1, 1, 1, 1, 1, 1, 0]
Cl	[1, 1, 1, 1, 1, 1, 1, 1, 0.5]
Ar	[1, 1, 1, 1, 1, 1, 1, 1, 1]

[atoms] \times 16 [length of array] \times 3 [dimensions]. \mathbf{e}_s and \mathbf{e}_v correspond to edge scalar and edge vector arrays. In addition, l_s and l_v are defined as the edge length scalar and vector. l_v contains the vectors of the edges, which are the bond distance vector between two atoms in Cartesian coordinates. l_s is calculated by $|l_v|$. l_s and l_v are constant values in a given structure. In this model, the edge is counted only when l_s is less than the cutoff length.

1. Input layer

At the input layer, \mathbf{n}_s corresponds to the element type. To imitate the occupancy of electron orbitals, the values corresponding to the atomic number are divided by 2 and packed by 1 from the top of the array. The list is shown in table IV. The input layer of edge scalar \mathbf{e}_s is calculated as

$$\mathbf{e}_s(l_s) = \exp(-\alpha l_s) + \alpha l_s + b, \quad (6)$$

where α is a network parameter. a and b are set to satisfy $\mathbf{e}_s(l_s)$ and its derivative $= 0$ when l_s equals to the cutoff distance. \mathbf{e}_s is expected to behave like the distance term of the Morse-style IP. Vector and tensor types of input values (\mathbf{n}_v , \mathbf{n}_t , and \mathbf{e}_v) are set to zero. It is noted that the input values of \mathbf{n}_s is the only place which depends on the element type.

2. Internal calculation of interaction block

Here, we write the linear layer (affine transformation layer) as $\text{lin}(\mathbf{x})$, the activation layer as $\text{act}(\mathbf{x})$, the concatenation function as $\text{con}(\mathbf{x}, \mathbf{y}, \dots)$, and the cutoff function as $\text{cut}(\mathbf{x})$. It is noted that each $\text{lin}(\mathbf{x})$ appeared in the following equations has different parameters. The detail of the activation function is described in section VI A 4. The cutoff function is a smoothly decaying function. In this work, we use the same function style as Eq. (6), but replacing $\exp(-\alpha x)$ by $\text{act}(x)$. The input values of a interaction block are \mathbf{n}_s , \mathbf{n}_v , \mathbf{n}_t , \mathbf{e}_s , and \mathbf{e}_v , where \mathbf{n}_s , \mathbf{n}_v , \mathbf{n}_t are node(atom) based scalars, vectors and tensors, and \mathbf{e}_s , \mathbf{e}_v are edge(bond) based scalars and vectors, respectively. The output values have the same shape as the input values. Each block also uses l_s and l_v as constant values.

Because the components of the vector and tensor values depend on the basis vectors of the coordination system, they should not be summed, multiplied, or combined with other values. Therefore, we applied the inner products of the vector values before combining them with scalar values. Moreover, the vector values are updated only through linear summations of them. The tensor values are treated in the same manner. They are created by the tensor product of two vectors. It should be noted that these operations are invariant to the rotation of the coordination system.

First, the node values and the edge values are transformed.

$$\begin{aligned}\mathbf{n}_{s1} &= \text{act}(\text{lin}(\text{con}(\mathbf{n}_s, |\mathbf{n}_v|))), \\ \mathbf{n}_{v1} &= \text{lin}(\mathbf{n}_v), \\ \mathbf{n}_{t1} &= \text{lin}(\mathbf{n}_t), \\ \mathbf{e}_{s1} &= \text{act}(\text{lin}(\text{con}(\mathbf{e}_s, |\mathbf{e}_v|))).\end{aligned}\tag{7}$$

Second, the node-type values are distributed to corresponding edges and various edge-type scalar values are calculated by taking the inner products of vector and tensor values. Here, we write the distributed node values with a hat like $\hat{\mathbf{n}}$. Exactly 2 node values are distributed to each edge, which is labeled as i and j below. It is noted that the sign of l_v depends on the order of i and j . Therefore, the sign should be inverted if l_v is used for the calculation labeled by i and j because of the order invariance. In addition, those values from nodes are multiplied by the cutoff function to ensure that all values of far-enough edges are 0.

$$\begin{aligned}\hat{\mathbf{n}}_{v2\{i,j\}} &= \hat{\mathbf{n}}_{v1\{i,j\}} \pm \hat{\mathbf{n}}_{t1\{i,j\}} \cdot l_v, \\ \mathbf{x}_{0\{i,j\}} &= \hat{\mathbf{n}}_{s1\{i,j\}} \text{cut}(l_s), \\ \mathbf{x}_{1\{i,j\}} &= \pm \hat{\mathbf{n}}_{v2\{i,j\}} \cdot l_v \text{cut}(l_s), \\ \mathbf{x}_{2\{i,j\}} &= \hat{\mathbf{n}}_{v2\{i,j\}} \cdot \mathbf{e}_v \text{cut}(l_s), \\ \mathbf{x}_3 &= \hat{\mathbf{n}}_{v2i} \cdot \hat{\mathbf{n}}_{v2j} \text{cut}(l_s).\end{aligned}\tag{8}$$

Third, these values are concatenated and the activation function is applied while maintaining the order invariance. \mathbf{y}_{tot} is considered to represent the state of the edge. It is noted that $\mathbf{x}_{0\{i,j\}}$, $\mathbf{x}_{1\{i,j\}}$, and $\mathbf{x}_{2\{i,j\}}$ depend on node label i and j . In this architecture, we use $\mathbf{x}_{0i} + \mathbf{x}_{0j}$ and $(\mathbf{x}_{0i} - \mathbf{x}_{0j})^2$ to maintain the order invariance.

$$\begin{aligned}\mathbf{y}_{\text{sym}} &= \text{lin}(\text{con}(\mathbf{x}_{0i} + \mathbf{x}_{0j}, \mathbf{x}_{1i} + \mathbf{x}_{1j}, \mathbf{x}_{2i} + \mathbf{x}_{2j}, \mathbf{x}_3, \mathbf{e}_{s1})), \\ \mathbf{y}_{\text{asym}} &= \text{lin}(\text{con}(\mathbf{x}_{0i} - \mathbf{x}_{0j}, \mathbf{x}_{1i} - \mathbf{x}_{1j}, \mathbf{x}_{2i} - \mathbf{x}_{2j})), \\ \mathbf{y}_{\text{tot}} &= \text{act}(\mathbf{y}_{\text{sym}}) + (\mathbf{y}_{\text{asym}})^2.\end{aligned}\tag{9}$$

where $(\mathbf{y}_{\text{asym}})^2$ means element-by-element square.

Fourth, node-type variables are calculated from \mathbf{y}_{tot} .

$$\begin{aligned}\hat{\mathbf{n}}_{s3\{i,j\}} &= \text{lin}(\mathbf{y}_{\text{tot}}), \\ \hat{\mathbf{n}}_{v3\{i,j\}} &= \text{lin}(\mathbf{y}_{\text{tot}})\mathbf{e}_{s1} \pm \text{lin}(\mathbf{y}_{\text{tot}})l_v, \\ \hat{\mathbf{n}}_{t3\{i,j\}} &= \text{lin}(\mathbf{y}_{\text{tot}})l_v \otimes l_v \pm \text{lin}(\mathbf{n}_v) \otimes l_v.\end{aligned}\tag{10}$$

These values are transferred to corresponding nodes by the summation layer shown in Fig. 1.

Finally, node and edge variables are updated by ResNet-style bypass function.

$$\begin{aligned}\mathbf{n}_{s4} &= \mathbf{n}_s + \text{lin}(\mathbf{n}_s) + \text{lin}(\mathbf{n}_s)\mathbf{n}_{s3}, \\ \mathbf{n}_{v4} &= \mathbf{n}_v + \text{lin}(\mathbf{n}_v) + \text{lin}(\mathbf{n}_s)\mathbf{n}_{v3}, \\ \mathbf{n}_{t4} &= \mathbf{n}_t + \text{lin}(\mathbf{n}_t) + \text{lin}(\mathbf{n}_s)\mathbf{n}_{t3} + \text{lin}(\mathbf{I}), \\ \mathbf{e}_{s4} &= \mathbf{e}_s + \text{lin}(\mathbf{e}_s) + \text{lin}(\mathbf{y}_{\text{tot}}), \\ \mathbf{e}_{v4} &= \mathbf{e}_v + \text{lin}(\mathbf{e}_v) + \text{lin}(\mathbf{y}_{\text{tot}})\text{lin}(\mathbf{y}_{\text{asym}})l_v + \text{lin}(\hat{\mathbf{n}}_{v2i} + \hat{\mathbf{n}}_{v2j}),\end{aligned}\tag{11}$$

where \mathbf{I} is the ideal tensor. A node convolution gate is also applied by multiplying $\text{lin}(\mathbf{n}_s)$. These variables are the final output of the interaction block and used as the input variables of the next block.

3. Output layer

At the end of the network, it is expected to output one scalar value. This is calculated by taking the summation of scalar arrays along with all nodes and edges.

$$E = \sum_{\text{nodes}} \text{lin}(\mathbf{n}_s) + \sum_{\text{edges}} \text{lin}(\mathbf{e}_s). \quad (12)$$

4. Activation function for double backpropagation

Although the intended output of the network is the energy of the system, the network is trained to simultaneously compute the atomic forces, providing useful data for training. The atomic forces are calculated by a backpropagation process, and the training process becomes a double backpropagation. The molecular dynamics simulation requires a smooth activation function. In this study, we employed the integral of the softplus function, which (to our knowledge) we were first to propose as an activation function. The integral is calculated as follows:

$$\begin{aligned} f(x) &= \int_{-\infty}^x \log(1 + \exp(t)) dt \\ &= -\text{Li}_2(-\exp(x)), \end{aligned} \quad (13)$$

where Li_2 is a second-order polylogarithm function. This function approaches 0 as x tends to $-\infty$ and approaches the curve of $x^2 + C$ at large x , where C is a constant. When this function is applied to the edge arrays, the activation functions are shifted so that $f(0)$ becomes 0. Using the activation function, we can train a softplus-type network in the second backpropagation process. If the polylogarithm function is replaced by the softplus function, the second backpropagation process results in a sigmoid-type network. The function shape is shown in Fig. 5. The effect of this change to the prediction accuracy is presented in the section III.

B. Data collection

The dataset is created as follows. First, the simulation box is filled with tens of atoms. The element type is randomly selected from the first three rows of the periodic table (from H to Ar). The number of element types and their ratio in one sample is also widely distributed. The system is heated to high temperature (e.g. 10,000 K), melted for approximately 100 femtoseconds, cooled to a setting temperature, then further annealed for another 100 femtoseconds by classical MD to obtain a snapshot. The timestep is 1 femtosecond. This process is repeated for various temperatures (up to 5,000 K) and volumes. Then, the reference energy and atomic forces are obtained by DFT calculations of the snapshots. We consider that

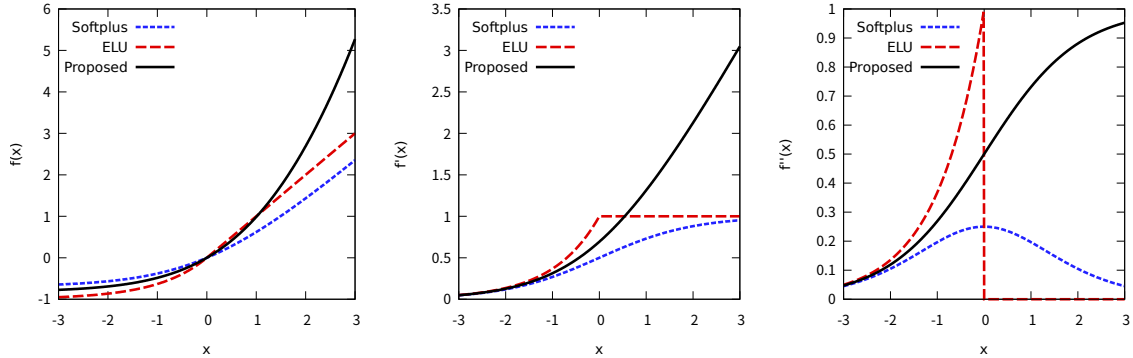


FIG. 5. Left: comparison of activation functions. Softplus and ELU ($\alpha = 1$) functions[48] are also shown. They are shifted so that $f(0)$ becomes 0. Middle: derivative of the activation functions. Right: second derivative of activation functions. In softplus and ELU, second gradient value $f''(x)$ vanishes when x is large.

this dataset consists of highly disordered structures, including many types of local atomic configurations, and thus presents a challenging task. Furthermore, most of the configurations are far from stable.

In addition, to include realistic structure, we create another dataset by heating the structures of the molecular dataset of the Materials Project repository [49] up to 3,000 K. In this work, we merged those two datasets. The entire dataset contains approximately 294,000 structures. The size of the dataset at the double backpropagation process (the corresponding atomic forces of the 294,000 structures) is approximately 7,375,000. Two-hundred randomly selected structures (including 4962×3 atomic force data) are used for the test dataset exclusively.

We use VASP for DFT calculation. GGA is used for the exchange-correlation energy. Spin polarization is considered.

C. Training procedure

The NN hyperparameters are set as follows. The length of the scalar node and edge arrays is set to be 128. The length of the vector node, rank-2 tensor node, and vector edge arrays is each set to 16. The cutoff distance is set to 6 Å. The minibatch size is 100.

The network is trained by optimizing the combined absolute loss function (energies and atomic forces) using the Adam optimizer [50]. As the number of layers increased, frequent fluctuations were observed in the training error. This instability may be explained, at least in part, by the roughness of the DFT-calculated potential energy surface, which is the ground truth of this task. Small atomic displacements, such as the approaching of two neighboring atoms, can potentially cause abrupt energy increases.

To resolve this problem, we constrained the parameters of all intermediate layers in the

network to the same values at the initial stage of the training, as described in section II B.

Finally, the models were trained by stochastic gradient descent with a small learning rate (0.1). The numbers of iterations were set to 450,000 (initial), 450,000 (main), and 20,000 (final) in all cases.

Note

The implementation for Chainer and the datasets will be available if this paper is accepted.

Acknowledgments

Acknowledgments will be inserted in the final version.

-
- [1] John Edward Jones. On the determination of molecular fields. —ii. from the equation of state of a gas. *Proceedings of the Royal Society of London A: Mathematical, Physical and Engineering Sciences*, 106(738):463–477, 1924.
 - [2] Murray S. Daw and M. I. Baskes. Embedded-atom method: Derivation and application to impurities, surfaces, and other defects in metals. *Phys. Rev. B*, 29:6443–6453, Jun 1984.
 - [3] Frank H. Stillinger and Thomas A. Weber. Computer simulation of local order in condensed phases of silicon. *Phys. Rev. B*, 31:5262–5271, Apr 1985.
 - [4] J. Tersoff. Modeling solid-state chemistry: Interatomic potentials for multicomponent systems. *Phys. Rev. B*, 39:5566–5568, Mar 1989.
 - [5] So Takamoto, Takahiro Yamasaki, Jun Nara, Takahisa Ohno, Chioko Kaneta, Asuka Hatano, and Satoshi Izumi. Atomistic mechanism of graphene growth on a sic substrate: Large-scale molecular dynamics simulations based on a new charge-transfer bond-order type potential. *Phys. Rev. B*, 97:125411, Mar 2018.
 - [6] Jörg Behler and Michele Parrinello. Generalized neural-network representation of high-dimensional potential-energy surfaces. *Phys. Rev. Lett.*, 98:146401, Apr 2007.
 - [7] Justin Gilmer, Samuel S Schoenholz, Patrick F Riley, Oriol Vinyals, and George E Dahl. Neural message passing for quantum chemistry. *arXiv preprint arXiv:1704.01212*, 2017.
 - [8] Kristof T Schütt, Farhad Arbabzadah, Stefan Chmiela, Klaus R Müller, and Alexandre Tkatchenko. Quantum-chemical insights from deep tensor neural networks. *Nature communications*, 8:13890, 2017.
 - [9] Kristof Schütt, Pieter-Jan Kindermans, Huziel Enoc Saucedo Felix, Stefan Chmiela, Alexandre Tkatchenko, and Klaus-Robert Müller. Schnet: A continuous-filter convolutional neural network for modeling quantum interactions. In *Advances in Neural Information Processing Systems*, pages 992–1002, 2017.

- [10] Mengyu Chu and Nils Thuerey. Data-driven synthesis of smoke flows with cnn-based feature descriptors. *ACM Trans. Graph.*, 36(4):69:1–69:14, July 2017.
- [11] Juan Carrasquilla and Roger G Melko. Machine learning phases of matter. *Nature Physics*, 13(5):431, 2017.
- [12] Giacomo Torlai, Guglielmo Mazzola, Juan Carrasquilla, Matthias Troyer, Roger Melko, and Giuseppe Carleo. Many-body quantum state tomography with neural networks. *arXiv preprint arXiv:1703.05334*, 2017.
- [13] F. Scarselli, M. Gori, A. C. Tsoi, M. Hagenbuchner, and G. Monfardini. The graph neural network model. *IEEE Transactions on Neural Networks*, 20(1):61–80, Jan 2009.
- [14] Michael M Bronstein, Joan Bruna, Yann LeCun, Arthur Szlam, and Pierre Vandergheynst. Geometric deep learning: going beyond euclidean data. *IEEE Signal Processing Magazine*, 34(4):18–42, 2017.
- [15] Aditya Grover, Aaron Zweig, and Stefano Ermon. Graphite: Iterative generative modeling of graphs. *arXiv preprint arXiv:1803.10459*, 2018.
- [16] MC Payne, MP Teter, DC Allan, TA Arias, and JD Joannopoulos. Iterative minimization techniques for abinitio total-energy calculations - molecular-dynamics and conjugate gradients. *Rev. Mod. Phys.*, 64:1045–1097, 1992.
- [17] W. Kohn and L. J. Sham. Self-consistent equations including exchange and correlation effects. *Phys. Rev.*, 140:A1133–A1138, Nov 1965.
- [18] XF Qian, J Li, L Qi, CZ Wang, TL Chan, YX Yao, KM Ho, and S Yip. Quasiatomic orbitals for ab initio tight-binding analysis. *Phys. Rev. B*, 78:245112, 2008.
- [19] CZ Wang, GD Lee, J Li, S Yip, and KM Ho. Atomistic simulation studies of complex carbon and silicon systems using environment-dependent tight-binding potentials. *Sci. Model. Simul.*, 15:97–121, 2008.
- [20] CZ Wang, WC Lu, YX Yao, J Li, S Yip, and KM Ho. Tight-binding hamiltonian from first-principles calculations. *Sci. Model. Simul.*, 15:81–95, 2008.
- [21] Anthony K. Rappe and William A. Goddard. Charge equilibration for molecular dynamics simulations. *The Journal of Physical Chemistry*, 95(8):3358–3363, 1991.
- [22] M. W. Finnis and J. E. Sinclair. A simple empirical n-body potential for transition metals. *Philosophical Magazine A*, 50(1):45–55, 1984.
- [23] LX He and D Vanderbilt. Exponential decay properties of wannier functions and related quantities. *Phys. Rev. Lett.*, 86:5341–5344, 2001.
- [24] Adri C. T. van Duin, Siddharth Dasgupta, Francois Lorant, and William A. Goddard. Reaxff: A reactive force field for hydrocarbons. *The Journal of Physical Chemistry A*, 105(41):9396–9409, 2001.
- [25] Jianguo Yu, Susan B. Sinnott, and Simon R. Phillpot. Charge optimized many-body potential for the Si/sio₂ system. *Phys. Rev. B*, 75:085311, Feb 2007.
- [26] So Takamoto, Tomohisa Kumagai, Takahiro Yamasaki, Takahisa Ohno, Chioko Kaneta, Asuka Hatano, and Satoshi Izumi. Charge-transfer interatomic potential for investigation of the thermal-oxidation growth process of silicon. *Journal of Applied Physics*, 120(16):165109, 2016.
- [27] Kaiming He, Xiangyu Zhang, Shaoqing Ren, and Jian Sun. Deep residual learning for image recognition. In *Proceedings of the IEEE conference on computer vision and pattern recognition*, pages 770–778, 2016.
- [28] Dongyoon Han, Jiwhan Kim, and Junmo Kim. Deep pyramidal residual networks. In *Computer Vision and Pattern Recognition (CVPR), 2017 IEEE Conference on*, pages 6307–6315. IEEE,

- 2017.
- [29] Sergey Zagoruyko and Nikos Komodakis. Wide residual networks. *arXiv preprint arXiv:1605.07146*, 2016.
 - [30] Saining Xie, Ross Girshick, Piotr Dollár, Zhuowen Tu, and Kaiming He. Aggregated residual transformations for deep neural networks. In *Computer Vision and Pattern Recognition (CVPR), 2017 IEEE Conference on*, pages 5987–5995. IEEE, 2017.
 - [31] Kaiming He, Georgia Gkioxari, Piotr Dollár, and Ross Girshick. Mask r-cnn. In *Computer Vision (ICCV), 2017 IEEE International Conference on*, pages 2980–2988. IEEE, 2017.
 - [32] Yonghui Wu, Mike Schuster, Zhifeng Chen, Quoc V Le, Mohammad Norouzi, Wolfgang Macherey, Maxim Krikun, Yuan Cao, Qin Gao, Klaus Macherey, et al. Google’s neural machine translation system: Bridging the gap between human and machine translation. *arXiv preprint arXiv:1609.08144*, 2016.
 - [33] Aaron Van Den Oord, Sander Dieleman, Heiga Zen, Karen Simonyan, Oriol Vinyals, Alex Graves, Nal Kalchbrenner, Andrew Senior, and Koray Kavukcuoglu. Wavenet: A generative model for raw audio. *arXiv preprint arXiv:1609.03499*, 2016.
 - [34] Yiping Lu, Aoxiao Zhong, Quanzheng Li, and Bin Dong. Beyond finite layer neural networks: Bridging deep architectures and numerical differential equations. *arXiv preprint arXiv:1710.10121*, 2017.
 - [35] Bo Chang, Lili Meng, Eldad Haber, Lars Ruthotto, David Begert, and Elliot Holtham. Reversible architectures for arbitrarily deep residual neural networks. In *Thirty-Second AAAI Conference on Artificial Intelligence*, 2018.
 - [36] Tian Qi Chen, Yulia Rubanova, Jesse Bettencourt, and David K Duvenaud. Neural ordinary differential equations. In *Advances in neural information processing systems*, pages 6571–6583, 2018.
 - [37] Oliver T. Unke and Markus Meuwly. Physnet: A neural network for predicting energies, forces, dipole moments, and partial charges. *Journal of Chemical Theory and Computation*, 15(6):3678–3693, 2019. PMID: 31042390.
 - [38] Linfeng Zhang, Jiequn Han, Han Wang, Roberto Car, and Weinan E. Deep potential molecular dynamics: A scalable model with the accuracy of quantum mechanics. *Phys. Rev. Lett.*, 120:143001, Apr 2018.
 - [39] J. Tersoff. New empirical approach for the structure and energy of covalent systems. *Phys. Rev. B*, 37:6991–7000, Apr 1988.
 - [40] Matthias Rupp, Alexandre Tkatchenko, Klaus-Robert Müller, and O. Anatole von Lilienfeld. Fast and accurate modeling of molecular atomization energies with machine learning. *Phys. Rev. Lett.*, 108:058301, Jan 2012.
 - [41] Raghunathan Ramakrishnan, Pavlo O Dral, Matthias Rupp, and O Anatole Von Lilienfeld. Quantum chemistry structures and properties of 134 kilo molecules. *Scientific data*, 1:140022, 2014.
 - [42] Shinji Munetoh, Teruaki Motooka, Koji Moriguchi, and Akira Shintani. Interatomic potential for si–o systems using tersoff parameterization. *Computational Materials Science*, 39(2):334–339, 2007.
 - [43] Johannes Sarnthein, Alfredo Pasquarello, and Roberto Car. Model of vitreous sio 2 generated by an ab initio molecular-dynamics quench from the melt. *Physical Review B*, 52(17):12690, 1995.

- [44] Alan K Soper. The radial distribution functions of water as derived from radiation total scattering experiments: Is there anything we can say for sure? *ISRN Physical Chemistry*, 2013, 2013.
- [45] William M Haynes. *CRC handbook of chemistry and physics*. CRC press, 2014.
- [46] Martin Neumann. Dipole moment fluctuation formulas in computer simulations of polar systems. *Molecular Physics*, 50(4):841–858, 1983.
- [47] Mauro Boero, Tamio Ikeshoji, and Kiyoyuki Terakura. Density and temperature dependence of proton diffusion in water: A first-principles molecular dynamics study. *ChemPhysChem*, 6(9):1775–1779, 2005.
- [48] Djork-Arné Clevert, Thomas Unterthiner, and Sepp Hochreiter. Fast and accurate deep network learning by exponential linear units (elus). *arXiv preprint arXiv:1511.07289*, 2015.
- [49] Anubhav Jain, Shyue Ping Ong, Geoffroy Hautier, Wei Chen, William Davidson Richards, Stephen Dacek, Shreyas Cholia, Dan Gunter, David Skinner, Gerbrand Ceder, and Kristin A. Persson. Commentary: The materials project: A materials genome approach to accelerating materials innovation. *APL Materials*, 1(1):011002, 2013.
- [50] Diederik P Kingma and Jimmy Ba. Adam: A method for stochastic optimization. *arXiv preprint arXiv:1412.6980*, 2014.

APPENDIX

1. The necessity of Rank-2 tensors and its physical meaning

Rank-2 tensors are essential to express the edge-edge interaction through their angle by graph convolution operation. This can be demonstrated in the following example. Let the nodes and edges contain only vector values, and suppose that two edges are connected to a center node, that has point-group symmetry as shown in Fig. 6. After the convolution, the summed vector values at the node are always $\mathbf{0}$, and the node loses its directional information. If the third edge is connected to the node, no angle dependence is represented. However, if the second-order tensor values are introduced, the point-group symmetric edge pairs have identical (no sign reversal) tensor values; therefore, the directional information can be accumulated on the node. It should be noted that the vector and tensor values are not merely mathematical tricks but express various physical quantities related to the electronic structure. For example, the local charge deviation is expressed by the electric dipole moment. Since the electron orbit of a π bond extends perpendicularly to the bond direction, the dihedral bending is prevented. Polarizability can be expressed by tensor as well. These properties can be naturally expressed using the vector and tensor variables. Higher-order tensor values can also be introduced in the same manner.

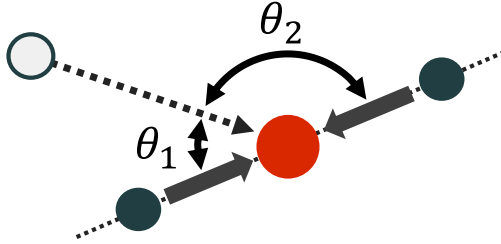


FIG. 6. Example of the vanishment of directional information when convoluting with vector values only. If a pair of atoms (shown in dark green circles) having the same properties are located on opposite sides of the center atom (shown in orange circle), any vector values summed at the center atom will vanish. Thus, the angular-dependent interaction between another neighbor atom (shown in white circle) and dark green atoms, corresponding to θ_1 and θ_2 , cannot be incorporated in the model.

2. Details of dataset

The details of the test dataset is shown. Since it was made by randomly selecting from the entire dataset, it can be considered to reflect the trend of the entire dataset.

Table V shows the amount of each element in the test dataset. The calculated energy is also shown. The structures of the first 20 samples in table V are shown in Fig. 7. Table VI shows the number of pairs in the test dataset. As described in the main text, the dataset consists of highly disordered structures.

TABLE V: Content of the test dataset. The number of each element in the test dataset is shown. E corresponds to the total energy of the system calculated by DFT. The zero point of the energy is defined as the sum of the energies of atoms separated in a vacuum. The unit of energy is eV.

	H	He	Li	Be	B	C	N	O	F	Ne	Na	Mg	Al	Si	P	S	Cl	Ar	E	E /atom
	0	1	1	0	0	3	0	1	3	1	0	0	3	0	0	1	2	2	-32.57	-1.81
	1	0	0	0	0	0	0	2	1	0	1	1	0	0	0	1	0	1	-22.14	-2.77
	0	1	1	1	2	2	0	2	2	1	0	1	2	0	1	0	0	0	-58.83	-3.68
	0	1	1	1	0	1	2	1	1	1	1	1	0	1	1	1	1	1	-53.44	-3.34
	0	0	8	0	0	0	0	0	0	0	0	0	8	0	0	0	0	0	-30.25	-1.89
	0	0	0	0	0	0	3	1	0	1	0	1	0	0	1	0	1	0	-18.42	-2.30
	0	0	0	0	1	1	2	0	4	0	0	1	2	1	2	0	1	1	-64.72	-4.05
	0	0	0	0	1	0	1	0	0	0	0	0	0	1	0	2	2	1	-22.55	-2.82
	0	0	0	0	0	0	0	0	0	9	9	0	0	0	0	0	0	0	0.97	0.05
	0	1	0	2	0	0	1	0	1	0	0	1	2	0	1	0	0	1	-25.22	-2.52
	0	0	0	0	0	0	0	0	0	2	0	0	0	1	1	0	0	0	-2.54	-0.63
	3	0	2	0	0	1	0	0	2	1	0	0	0	1	3	1	2	0	-47.47	-2.97
	0	0	1	0	1	0	0	1	1	2	1	4	1	1	0	0	0	3	-26.56	-1.66
	0	0	4	0	0	0	0	0	0	4	0	0	0	0	0	0	0	0	-2.99	-0.37
	2	0	2	0	1	3	0	1	0	0	0	1	1	1	3	0	0	1	-55.86	-3.49
16	0	0	0	0	0	0	0	0	32	0	16	0	0	0	0	0	0	0	-197.82	-3.09
9	6	10	12	7	12	9	3	7	9	6	10	5	3	3	7	6	4	4	-394.97	-3.09
	0	0	9	0	0	0	0	9	0	0	0	0	0	0	0	0	0	0	-62.79	-3.49
	0	0	0	2	0	1	1	0	1	0	0	2	0	0	0	1	0	0	-23.62	-2.95
	0	0	1	0	1	0	0	0	0	0	0	0	0	0	0	0	14	0	-28.70	-1.79
	0	0	8	0	0	0	0	0	8	0	0	0	0	0	0	0	0	0	-58.89	-3.68
	2	0	3	1	1	1	1	0	2	0	0	0	3	0	1	1	0	0	-48.22	-3.01
	1	2	2	0	0	1	1	1	0	0	0	3	1	0	0	0	2	2	-27.45	-1.72
	2	1	2	1	0	0	0	0	3	3	0	0	2	0	1	1	0	0	-41.19	-2.57
	0	0	0	0	0	1	0	0	0	0	0	0	0	0	0	0	0	7	1.25	0.16
	0	0	0	0	0	0	0	0	0	1	0	15	0	0	0	0	0	0	-0.22	-0.01
	0	0	16	0	0	0	0	0	0	0	0	0	0	0	0	0	0	0	-28.89	-1.81
10	0	0	0	0	0	12	2	0	0	0	0	0	0	0	0	0	0	0	-117.52	-4.90

H	He	Li	Be	B	C	N	O	F	Ne	Na	Mg	Al	Si	P	S	Cl	Ar	E	E /atom
1	1	0	2	1	0	1	2	1	0	2	1	1	1	1	0	1	0	-56.39	-3.52
1	1	0	0	1	0	1	1	1	0	0	0	0	1	2	0	1	0	-36.41	-3.64
1	1	1	0	2	1	0	0	2	1	2	1	0	2	1	1	1	1	-45.35	-2.52
0	3	1	0	0	0	1	3	0	1	0	2	0	0	1	2	2	0	-36.98	-2.31
2	0	2	2	0	2	0	0	1	2	2	0	2	1	2	0	0	2	-34.90	-1.74
0	0	0	0	0	0	0	0	0	9	0	0	0	0	9	0	0	0	-20.54	-1.14
0	0	0	0	1	0	1	1	0	1	0	2	0	1	0	0	1	0	-22.94	-2.87
4	1	2	2	0	0	1	1	1	0	1	1	1	0	1	0	0	0	-35.49	-2.22
1	1	0	1	2	1	1	0	0	1	2	0	1	1	1	2	0	3	-32.36	-1.80
1	0	1	0	0	2	1	0	0	0	1	0	0	0	0	2	0	0	-25.29	-3.16
4	5	2	2	4	5	3	5	1	6	2	4	1	2	2	9	5	2	-220.63	-3.45
0	2	1	1	1	1	0	0	1	1	0	1	0	1	0	0	0	0	-23.16	-2.32
2	0	0	0	0	0	0	1	0	2	0	0	0	0	0	0	2	1	-10.70	-1.34
0	0	0	0	2	0	0	0	0	0	0	0	0	0	0	0	0	0	-3.60	-1.80
1	2	0	0	0	2	2	2	1	1	0	1	1	0	1	0	2	0	-60.44	-3.78
1	2	0	0	0	1	0	0	0	1	0	0	1	0	1	1	0	0	-11.70	-1.46
0	0	0	0	0	0	0	0	0	0	0	0	0	0	0	10	10	0	-41.19	-2.06
0	0	15	0	0	0	0	0	0	0	1	0	0	0	0	0	0	0	-31.25	-1.95
0	0	2	2	0	1	1	0	0	0	0	2	3	0	0	1	3	1	-44.95	-2.81
0	0	0	0	4	0	0	0	0	0	4	0	0	0	0	0	0	0	-21.54	-2.69
0	0	0	0	1	0	1	1	0	0	1	0	1	1	0	1	1	0	-26.63	-3.33
0	0	0	0	0	0	0	0	0	8	0	8	0	0	0	0	0	0	-5.74	-0.36
1	0	0	0	1	0	1	0	0	1	0	0	2	1	0	0	1	0	-10.77	-1.35
1	0	0	1	0	2	0	0	1	0	0	0	1	0	1	0	0	1	-25.65	-3.21
1	1	0	1	0	1	2	1	2	0	0	1	0	1	0	0	0	1	-46.32	-3.86
5	5	4	4	3	3	3	6	3	4	4	1	5	1	0	3	4	6	-206.37	-3.22
0	0	0	0	0	16	0	0	0	0	0	0	0	0	0	0	0	0	-22.43	-1.40
0	0	0	0	0	0	0	0	0	0	4	0	0	4	0	0	0	0	-16.87	-2.11
6	0	10	0	0	0	0	0	0	0	0	0	0	0	4	0	0	0	-36.95	-1.85
0	0	0	0	1	0	1	0	0	0	0	0	0	2	0	0	0	0	-13.41	-3.35
2	0	1	0	1	1	1	0	1	0	1	0	1	1	0	1	1	0	-34.68	-2.89
0	0	0	0	0	0	0	0	0	0	0	0	9	0	0	0	9	0	-45.46	-2.53
0	0	0	0	0	0	8	0	0	8	0	0	0	0	0	0	0	0	-41.27	-2.58
0	2	2	2	1	0	2	1	1	2	0	0	1	1	0	0	1	0	-43.28	-2.71
0	0	0	0	8	0	0	0	8	0	0	0	0	0	0	0	0	0	-80.56	-5.03
0	1	2	1	0	0	0	2	0	0	0	0	0	0	0	2	0	0	-24.73	-3.09
0	0	0	0	0	0	0	0	0	1	0	0	0	0	0	1	1	1	-1.31	-0.33
0	2	1	0	2	1	0	3	1	1	0	0	2	1	1	1	2	2	-61.66	-3.08
0	0	0	0	0	0	0	1	0	0	0	0	0	2	0	0	0	1	-10.50	-2.62
0	0	0	9	0	0	9	0	0	0	0	0	0	0	0	0	0	0	-71.42	-3.97
2	0	0	0	0	1	1	1	0	0	1	0	1	0	2	2	1	4	-42.65	-2.67
0	3	1	3	0	0	0	0	1	0	0	2	2	0	2	1	1	0	-39.80	-2.49
1	0	1	1	0	0	0	1	0	0	2	0	0	1	0	1	0	0	-22.08	-2.76

H	He	Li	Be	B	C	N	O	F	Ne	Na	Mg	Al	Si	P	S	Cl	Ar	E	E /atom
5	6	7	10	8	12	14	2	9	10	5	6	3	8	6	9	3	5	-427.13	-3.34
0	0	0	0	0	0	0	0	1	0	0	6	0	0	0	0	1	0	-15.13	-1.89
0	0	0	0	16	0	0	0	0	0	0	0	0	0	0	0	0	0	-88.14	-5.51
2	1	1	1	0	1	1	0	2	1	3	0	0	1	0	1	0	1	-39.07	-2.44
0	0	0	1	1	0	0	2	2	0	1	1	1	0	3	0	0	0	-42.05	-3.50
1	1	2	2	3	0	0	0	0	0	1	1	0	0	0	2	2	1	-39.07	-2.44
0	1	1	1	1	0	0	3	0	1	0	0	1	1	0	0	0	0	-32.15	-3.22
8	0	0	0	0	8	0	0	0	0	0	0	0	0	0	0	0	0	-71.87	-4.49
1	0	1	1	0	3	5	0	1	0	1	1	1	1	1	1	1	1	-66.54	-3.33
1	1	3	1	0	0	1	2	0	1	1	0	0	2	0	1	1	1	-46.73	-2.92
0	1	0	1	0	2	1	1	0	0	1	1	0	0	0	2	1	1	-38.19	-3.18
0	2	1	1	1	1	1	0	2	0	0	1	1	1	0	1	0	3	-46.10	-2.88
0	0	8	0	16	0	8	16	8	8	0	0	16	0	32	8	8	0	-461.06	-3.60
0	0	0	0	0	0	0	0	0	0	0	0	15	0	0	1	0	0	-44.16	-2.76
11	8	8	6	8	11	6	3	5	12	9	6	6	6	6	4	6	7	-374.90	-2.93
0	0	0	0	0	0	0	0	0	0	0	0	16	0	0	0	0	0	-39.70	-2.48
6	0	0	0	0	8	2	0	0	0	0	0	0	0	0	0	0	0	-75.53	-4.72
1	0	0	1	0	1	1	0	2	0	0	0	2	3	1	2	0	2	-56.83	-3.55
1	1	0	0	0	0	1	2	2	1	1	0	0	0	0	2	5	0	-32.44	-2.03
0	0	1	1	1	0	1	0	0	1	2	0	0	0	0	0	0	1	-7.19	-0.90
0	0	0	0	0	0	8	0	0	0	0	0	0	0	0	0	0	0	-40.96	-5.12
0	2	0	1	0	1	1	1	0	1	0	1	2	1	1	0	4	0	-37.51	-2.34
0	0	0	10	0	10	0	0	0	0	0	0	0	0	0	0	0	0	-93.71	-4.69
1	2	3	1	0	1	1	0	0	2	1	1	0	2	0	2	2	1	-44.09	-2.20
4	0	0	0	0	4	2	2	0	0	0	0	0	0	0	0	0	0	-51.94	-4.33
0	0	0	1	2	0	3	0	1	0	0	1	0	1	2	1	0	0	-53.71	-4.48
0	0	0	0	0	0	0	0	0	4	0	0	0	4	0	0	0	0	-11.15	-1.39
0	1	0	0	0	2	1	3	1	2	0	3	0	1	0	0	0	2	-50.47	-3.15
0	0	8	0	0	0	0	8	0	0	0	0	0	0	0	0	0	0	-57.67	-3.60
2	2	0	1	2	1	0	0	0	1	1	0	1	2	0	0	1	2	-29.53	-1.85
14	7	4	0	2	5	13	8	8	7	5	10	5	9	11	7	7	6	-378.64	-2.96
0	0	0	0	0	9	0	0	0	0	0	0	0	0	0	9	0	0	-74.44	-4.14
0	1	0	0	0	0	0	0	7	0	0	0	0	0	0	0	0	0	-6.89	-0.86
0	0	0	0	0	0	9	0	0	0	9	0	0	0	0	0	0	0	-46.17	-2.56
4	7	7	4	4	4	7	3	0	5	2	3	3	3	2	2	3	1	-204.67	-3.20
0	0	0	0	0	0	0	1	0	0	0	0	0	0	0	0	1	6	-2.18	-0.27
0	4	0	0	0	0	0	0	0	0	0	0	0	0	4	4	0	4	-19.82	-1.24
3	3	1	1	1	2	2	3	3	33	2	3	1	1	2	0	0	3	-92.94	-1.45
1	3	1	2	0	2	2	1	1	0	1	1	0	1	0	2	0	2	-51.51	-2.58
0	0	0	1	2	1	2	0	0	0	2	2	2	3	1	0	0	0	-59.71	-3.73
16	8	16	0	0	0	8	8	0	24	0	0	24	8	0	0	8	8	-266.13	-2.08
2	2	1	1	0	1	0	1	0	0	0	1	1	0	3	2	0	1	-45.98	-2.87
0	2	0	0	0	0	0	0	0	0	0	0	0	0	16	0	0	0	-44.08	-2.45

H	He	Li	Be	B	C	N	O	F	Ne	Na	Mg	Al	Si	P	S	Cl	Ar	E	E /atom
0	1	0	0	2	0	1	0	1	2	0	2	0	1	2	0	0	0	-24.05	-2.00
0	0	0	0	0	0	0	0	0	0	0	0	0	0	0	16	0	0	-47.83	-2.99
8	8	2	8	8	6	10	2	7	8	7	3	11	6	5	9	14	6	-383.19	-2.99
0	0	0	0	8	0	0	0	0	0	0	0	0	0	0	8	0	0	-76.73	-4.80
0	0	2	1	3	1	0	2	1	1	0	0	0	1	1	1	0	2	-59.94	-3.75
0	0	0	0	7	0	1	0	0	0	0	0	0	0	0	0	0	0	-33.89	-4.24
1	0	3	2	1	1	1	0	1	1	0	0	0	0	0	0	1	0	-29.74	-2.48
0	1	0	0	0	0	0	0	0	6	0	0	0	0	1	0	0	0	-0.06	-0.01
7	0	0	0	0	7	0	1	0	0	0	0	0	0	0	1	3	0	-74.36	-3.91
1	0	1	2	2	1	1	0	1	0	1	1	2	2	1	1	1	2	-54.96	-2.75
0	8	0	0	0	0	0	0	0	0	0	0	0	0	0	8	0	0	-22.66	-1.42
0	0	0	0	2	1	1	1	0	1	0	2	1	1	0	0	1	1	-31.12	-2.59
0	0	1	0	0	0	0	1	0	0	1	0	0	0	0	0	0	0	-5.95	-1.98
0	0	0	0	0	0	0	0	0	0	9	0	0	0	0	0	9	0	-47.85	-2.66
0	0	2	0	1	2	0	0	0	1	2	1	2	1	1	2	1	0	-52.83	-3.30
7	0	0	0	0	0	9	4	0	0	0	0	0	0	0	0	0	0	-60.71	-3.04
0	2	2	0	2	0	1	2	5	2	0	0	0	0	1	0	0	1	-49.48	-2.75
1	2	1	0	1	0	2	1	0	0	0	0	2	1	0	0	1	0	-40.21	-3.35
0	0	16	0	0	0	8	0	8	0	0	8	0	8	0	0	16	0	-185.75	-2.90
1	2	0	2	1	1	1	3	0	2	0	1	2	1	2	0	0	1	-61.69	-3.08
0	0	0	0	0	8	0	0	0	0	0	0	0	0	0	0	8	0	-59.34	-3.71
0	2	0	0	1	0	0	1	2	1	1	0	2	0	1	1	3	1	-42.74	-2.67
1	0	0	1	0	0	1	3	1	1	2	2	0	0	1	0	1	2	-37.49	-2.34
3	0	1	0	0	1	0	0	0	1	0	1	1	0	2	2	4	0	-39.57	-2.47
0	2	0	0	1	2	2	0	0	1	0	2	0	1	0	0	0	1	-33.80	-2.82
0	0	0	0	1	0	0	0	0	0	0	0	0	0	0	0	15	0	-29.37	-1.84
0	0	0	0	8	0	0	0	0	8	0	0	0	0	0	0	0	0	-39.13	-2.45
1	2	0	2	0	0	1	1	1	0	0	2	0	1	0	2	1	2	-45.19	-2.82
0	0	16	0	16	0	0	0	0	0	0	0	0	16	0	0	0	16	-170.52	-2.66
0	8	8	8	16	8	24	8	0	8	16	8	0	8	8	0	0	0	-483.13	-3.77
13	0	0	0	0	7	1	1	0	0	0	0	0	0	0	0	0	0	-88.00	-4.00
0	1	0	0	2	4	0	0	0	1	2	1	1	3	0	1	0	0	-56.86	-3.55
9	0	0	0	0	0	0	0	0	0	0	0	0	0	9	0	0	0	-38.97	-2.17
0	0	0	2	1	0	1	0	1	1	2	0	1	0	1	1	0	1	-33.08	-2.76
0	1	0	1	0	1	1	0	0	0	0	1	0	0	1	0	0	2	-17.18	-2.15
0	0	1	1	3	1	0	0	2	0	3	1	1	0	1	1	1	2	-45.47	-2.53
0	0	0	0	0	0	0	0	0	0	0	0	0	0	9	9	0	0	-45.55	-2.53
0	0	0	0	1	1	0	0	0	0	0	0	0	2	2	0	0	2	-12.91	-1.61
0	2	0	0	1	1	1	1	1	1	1	3	0	0	1	1	1	1	-44.00	-2.75
9	8	9	8	7	10	8	8	4	6	2	7	8	6	5	10	8	5	-370.09	-2.89
0	0	9	0	0	0	0	0	0	0	0	9	0	0	0	0	0	0	-11.95	-0.66
1	0	1	1	2	0	0	0	1	0	0	0	0	0	0	1	1	0	-24.14	-3.02
0	0	0	0	18	0	0	0	0	0	0	0	0	0	0	0	0	2	-83.57	-4.18

H	He	Li	Be	B	C	N	O	F	Ne	Na	Mg	Al	Si	P	S	Cl	Ar	E	E /atom
0	0	4	0	0	0	0	0	4	0	0	0	0	0	0	0	0	0	-31.34	-3.92
0	0	0	0	0	16	0	0	0	0	0	0	32	0	0	0	16	0	-248.64	-3.88
0	6	0	0	0	0	0	0	0	0	0	0	0	1	0	0	1	0	-3.70	-0.46
1	1	0	0	0	0	0	0	0	1	1	0	0	1	0	1	0	2	-7.90	-0.99
1	2	2	0	1	1	2	1	1	0	0	0	0	4	0	3	2	0	-59.84	-2.99
0	0	1	1	0	0	0	1	1	0	1	0	0	2	1	0	0	0	-27.50	-3.44
0	2	0	0	1	2	1	1	0	1	1	2	2	2	0	0	1	0	-37.31	-2.33
0	1	0	0	0	0	0	0	0	0	0	1	0	0	0	6	0	0	-19.17	-2.40
0	1	0	2	2	2	0	1	1	1	1	0	2	1	1	1	0	0	-56.88	-3.55
8	0	0	0	0	0	0	8	0	0	0	0	0	0	0	0	0	0	-49.09	-3.07
0	0	1	0	1	1	2	1	1	2	0	0	2	1	0	1	1	2	-49.73	-3.11
0	0	2	1	1	0	1	1	0	1	2	1	0	2	1	1	0	2	-42.56	-2.66
0	0	0	0	0	0	0	18	0	2	0	0	0	0	0	0	0	0	-57.64	-2.88
1	1	0	0	1	1	1	0	2	3	0	0	2	0	1	1	1	1	-39.10	-2.44
0	0	0	4	0	0	0	0	0	0	8	0	4	0	0	0	0	0	-18.93	-1.18
0	0	8	16	16	8	8	16	8	16	0	0	8	16	0	0	0	8	-484.78	-3.79
8	8	0	0	0	16	0	16	0	0	8	16	16	0	0	16	16	8	-414.13	-3.24
0	0	0	0	15	0	0	0	0	0	0	1	0	0	0	0	0	0	-81.78	-5.11
0	2	0	1	0	0	0	2	0	2	0	2	0	2	0	1	3	1	-34.70	-2.17
1	0	3	1	0	0	1	1	0	1	3	1	0	1	1	0	2	2	-35.55	-1.98
0	0	1	0	0	0	0	2	0	0	0	3	3	1	2	2	2	0	-50.47	-3.15
0	0	0	0	0	0	0	0	0	0	0	0	0	0	0	15	1	0	-43.11	-2.69
0	0	0	32	0	0	0	0	0	0	0	0	0	32	0	0	0	0	-230.94	-3.61
5	6	6	7	6	6	7	9	5	13	8	5	12	7	3	5	8	10	-326.74	-2.55
1	0	1	0	2	0	2	2	0	1	4	0	1	1	1	1	1	0	-51.42	-2.86
0	8	0	16	8	0	0	0	0	0	0	0	8	0	0	8	8	8	-138.38	-2.16
0	3	0	0	3	3	3	2	2	4	1	0	0	0	6	1	1	3	-68.00	-2.13
0	0	0	0	0	0	0	0	0	0	0	0	0	32	0	0	32	0	-219.32	-3.43
0	0	0	0	64	0	0	64	0	0	0	0	0	0	0	0	0	0	-796.72	-6.22
1	3	0	2	1	1	1	1	3	0	0	0	1	0	1	0	1	0	-51.38	-3.21
1	0	1	1	1	0	3	0	0	0	0	0	0	1	0	2	0	0	-41.80	-4.18
0	8	16	0	0	8	0	8	0	0	8	16	0	0	0	0	0	0	-130.89	-2.05
0	0	0	0	0	0	0	0	8	0	0	0	0	0	0	8	0	0	-45.30	-2.83
1	0	1	0	0	1	0	0	1	2	2	1	0	0	2	0	2	3	-35.13	-2.20
0	0	0	0	0	0	0	0	0	10	10	0	0	0	0	0	0	0	-7.75	-0.39
1	0	0	3	0	0	0	0	1	0	0	1	0	1	0	0	1	0	-14.94	-1.87
0	8	8	8	8	0	0	0	0	0	0	8	8	8	0	8	0	0	-148.50	-2.32
0	0	0	0	0	0	0	0	4	0	0	0	0	0	4	0	0	0	-24.20	-3.02
1	0	0	1	0	0	1	1	1	1	0	1	0	0	0	0	0	1	-13.42	-1.68
0	0	0	10	0	0	0	6	0	4	0	0	0	0	0	0	0	0	-75.76	-3.79
0	0	4	0	0	0	0	0	0	0	0	0	4	0	0	0	0	0	-17.00	-2.13
0	1	1	1	0	0	0	1	0	1	2	1	0	2	1	3	1	1	-42.95	-2.68

H	He	Li	Be	B	C	N	O	F	Ne	Na	Mg	Al	Si	P	S	Cl	Ar	E	E /atom
0	0	1	1	1	0	1	1	0	0	1	2	2	1	0	0	0	1	-27.97	-2.33

TABLE VI. The number of atom pairs in the test dataset.

	H	He	Li	Be	B	C	N	O	F	Ne	Na	Mg	Al	Si	P	S	Cl	Ar
H	981	403	622	300	277	916	684	1002	564	535	438	327	537	341	741	401	469	372
He		455	582	554	518	594	601	527	401	637	384	598	586	477	500	780	539	501
Li			2091	522	705	543	697	1313	662	676	509	902	741	802	502	432	779	460
Be				1208	671	766	929	590	401	606	414	411	621	1391	283	491	385	442
B					3324	505	739	3514	659	886	459	474	625	824	572	751	448	551
C						1333	681	538	393	554	477	599	841	460	396	868	676	490
N							1068	759	536	927	825	586	525	678	576	433	622	416
O								2745	387	758	404	520	625	462	505	414	506	455
F									815	499	520	369	402	415	488	519	503	372
Ne										1201	717	588	668	621	778	350	498	553
Na											741	451	374	393	295	346	527	321
Mg												917	468	489	302	482	630	383
Al													1515	516	475	599	1106	510
Si														1098	297	412	889	451
P															1155	716	408	342
S																1600	738	464
Cl																	1413	469
Ar																		421

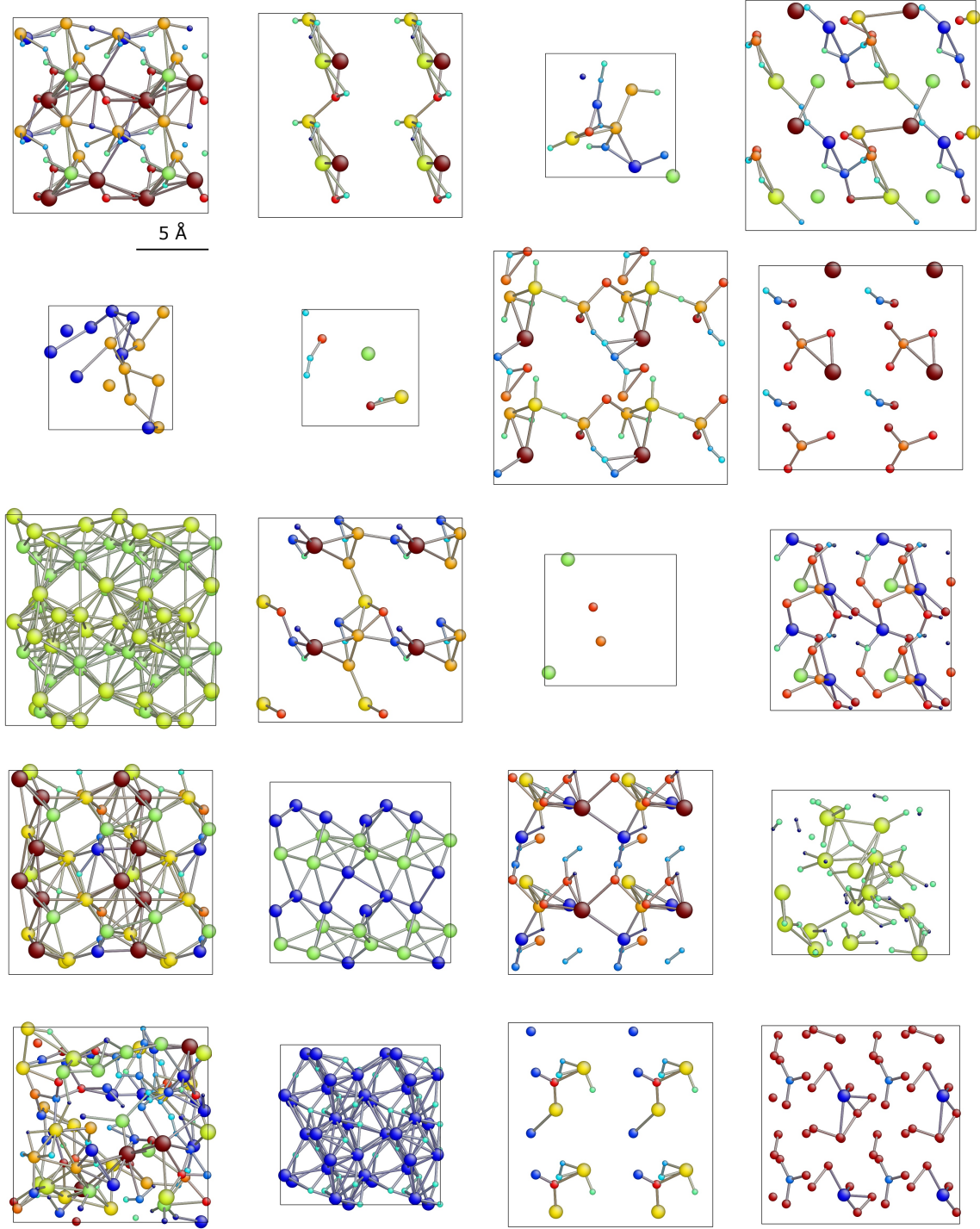


FIG. 7. The structures of the first 20 samples in table V are shown (order: top left to right). The colors of the atoms correspond to the element number (H: blue, Ar: red). It is noted that the structures with small box are drawn at a size of 2×2 . See table V for the details of component.